NAVAL POSTGRADUATE SCHOOL

MONTEREY, CALIFORNIA

THESIS

DOUBLE–DIFFUSIVE INTRUSIONS: DYNAMICS AND TRANSPORT

by

Gabriel A. Rosa

March 2022

Thesis Advisor: Timour Radko
Co-Advisor: Justin M. Brown

THIS PAGE INTENTIONALLY LEFT BLANK

REPORT DOCUMENTATION PAGE			Form Approved OMB No. 0704-0188

1. AGENCY USE ONLY *(Leave blank)*	**2. REPORT DATE** March 2022	**3. REPORT TYPE AND DATES COVERED** Master's thesis

4. TITLE AND SUBTITLE
DOUBLE–DIFFUSIVE INTRUSIONS: DYNAMICS AND TRANSPORT

5. FUNDING NUMBERS

6. AUTHOR(S) Gabriel A. Rosa

7. PERFORMING ORGANIZATION NAME(S) AND ADDRESS(ES)
Naval Postgraduate School
Monterey, CA 93943-5000

8. PERFORMING ORGANIZATION REPORT NUMBER

9. SPONSORING / MONITORING AGENCY NAME(S) AND ADDRESS(ES)
N/A

10. SPONSORING / MONITORING AGENCY REPORT NUMBER

11. SUPPLEMENTARY NOTES The views expressed in this thesis are those of the author and do not reflect the official policy or position of the Department of Defense or the U.S. Government.

12a. DISTRIBUTION / AVAILABILITY STATEMENT
Approved for public release. Distribution is unlimited.

12b. DISTRIBUTION CODE
A

13. ABSTRACT (maximum 200 words)

Intrusions are found throughout the ocean and are suspected to significantly transport salt, heat, nutrients, and pollutants laterally in ways that can have large impacts on large-scale ocean circulation. We perform the first fully resolved simulations that allow for the natural development of intrusions at an arbitrary inclination. This allows us to characterize their small-scale mixing and their lateral transport. We use these results to develop a less computationally expensive model that parameterizes the small-scale mixing of microscale double-diffusive processes in a multi-dimensional simulation. Such studies have been limited to one-dimensional simulations in the past. We test this parameterized model by comparing the results to a comparable fully resolved simulation. This allows us to perform simulations on more physically relevant scales for intrusions, which will allow us to explore the dependencies of heat and salt transport on our governing parameters of density ratio, aspect ratio, and isothermal slope. We find that intrusion-driven transport decreases with increasing density ratio and that the results depend strongly on the aspect ratio of the domain. Both fully resolved simulations and some parameterized simulations are dominated by collective instabilities. However, other parameterized simulations, particularly those at low density ratios, show the development of direct mode intrusions, and they evolve into thermohaline staircases.

14. SUBJECT TERMS double diffusion, intrusions, density ratio, thermohaline intrusions, crossfront intrusion, ocean convention, ocean circulation, salt-fingers, molecular diffusivity, collective instabilities	**15. NUMBER OF PAGES** 59
	16. PRICE CODE

17. SECURITY CLASSIFICATION OF REPORT	**18. SECURITY CLASSIFICATION OF THIS PAGE**	**19. SECURITY CLASSIFICATION OF ABSTRACT**	**20. LIMITATION OF ABSTRACT**
Unclassified	Unclassified	Unclassified	UU

NSN 7540-01-280-5500

Standard Form 298 (Rev. 2-89)
Prescribed by ANSI Std. 239-18

THIS PAGE INTENTIONALLY LEFT BLANK

Approved for public release. Distribution is unlimited.

DOUBLE–DIFFUSIVE INTRUSIONS: DYNAMICS AND TRANSPORT

Gabriel A. Rosa
Lieutenant, United States Navy
BE, State University of New York Maritime College, 2014

Submitted in partial fulfillment of the
requirements for the degree of

MASTER OF SCIENCE IN PHYSICAL OCEANOGRAPHY

from the

NAVAL POSTGRADUATE SCHOOL
March 2022

Approved by: Timour Radko
Advisor

Justin M. Brown
Co-Advisor

Peter C. Chu
Chair, Department of Oceanography

THIS PAGE INTENTIONALLY LEFT BLANK

ABSTRACT

Intrusions are found throughout the ocean and are suspected to significantly transport salt, heat, nutrients, and pollutants laterally in ways that can have large impacts on large-scale ocean circulation. We perform the first fully resolved simulations that allow for the natural development of intrusions at an arbitrary inclination. This allows us to characterize their small-scale mixing and their lateral transport. We use these results to develop a less computationally expensive model that parameterizes the small-scale mixing of microscale double-diffusive processes in a multi-dimensional simulation. Such studies have been limited to one-dimensional simulations in the past. We test this parameterized model by comparing the results to a comparable fully resolved simulation. This allows us to perform simulations on more physically relevant scales for intrusions, which will allow us to explore the dependencies of heat and salt transport on our governing parameters of density ratio, aspect ratio, and isothermal slope. We find that intrusion-driven transport decreases with increasing density ratio and that the results depend strongly on the aspect ratio of the domain. Both fully resolved simulations and some parameterized simulations are dominated by collective instabilities. However, other parameterized simulations, particularly those at low density ratios, show the development of direct mode intrusions, and they evolve into thermohaline staircases.

THIS PAGE INTENTIONALLY LEFT BLANK

TABLE OF CONTENTS

THIS PAGE INTENTIONALLY LEFT BLANK

LIST OF FIGURES

THIS PAGE INTENTIONALLY LEFT BLANK

LIST OF TABLES

THIS PAGE INTENTIONALLY LEFT BLANK

LIST OF ACRONYMS AND ABBREVIATIONS

2D	two-dimensional
3D	three-dimensional
DDC	double-diffusive convection
DNS	direct number simulation
MATLAB	matrix laboratory
Nu	Nusselt number
PADDI	PArallel Double DIffusion code
Pr	Prandtl number
Ra	Rayleighs number
Ri	Richardson number
F_S	salinity buoyancy flux
F_T	temperature buoyancy flux
$F_{S,H}$	salinity horizontal flux
$F_{T,H}$	temperature horizontal flux
A	aspect ratio
R_ρ	Density Ratio
G	Isotherm/isohaline Slopes
$\overline{F_T}$	averaged temperature buoyancy flux
$\overline{F_S}$	averaged salinity buoyancy flux
$\overline{F_{T,H}}$	averaged temperature horizontal flux
γ	flux ratio
γ^{-1}	inverse flux ratio
R_ρ	density ratio

THIS PAGE INTENTIONALLY LEFT BLANK

I. INTRODUCTION

Thermohaline intrusions have drawn a lot of interest from oceanographers from around the world since their introduction by Stern (1967). Thermohaline intrusions are laterally interleaving layers that have distinct temperature and salinity signatures. They can spontaneously form in fluids which are stratified both vertically and horizontally in temperature and salinity, which is common in the thermocline, where steep vertical gradients of temperature exist in the presence of weak horizontal gradients. Intrusions exist at vertical scales of 10m and horizontal scales of 1000m and can induce substantial lateral transport in the ocean. Intrusions have been studied in the laboratory (Thorpe et al. 1969; Ruddick et al. 1999; Krishnamurti 2009; Tanny and Tsinober 1988; Huppert and Turner 1980), in ocean observations (Joyce et al. 1978; Williams 1981; Schmitt and Georgi 1982), and in numerical experiments (Simeonov and Stern 2007; Hebert 2011).

A. MOTIVATION

The primary motivation behind the study of intrusions is to characterize their transport as it has consequences for the mixing of nutrients, heat, pollutants, and salinity throughout the ocean. Intrusions provide transport, through lateral and vertical mixing, of nutrient-rich ocean waters to regions with micro-organisms and other life (see, for example, a study of intrusions in the Canadian Basin by Mclaughlin et al. 2003). Though intrusions show substantial potential for lateral mixing in the ocean, the effects of that mixing on large-scale circulation are largely uncharacterized. Such is not the case for other forms of double-diffusive instabilities; for example, Merryfield et al. (1999) and Glessmer et al. (2008) showed that microscale double-diffusive instabilities substantially affect the strength of the thermohaline circulation. This would suggest that intrusions, which have substantially more lateral mixing than salt fingers or diffusive convection, could likely play a role in the thermohaline circulation. However, this proposition has received only limited attention in the literature, and most recent studies on this subject, such as Rudels et al. (2009) and Walsh and Carmack (2002), are largely qualitative. It would be prudent for

future models to expand upon their existing microscale mixing models to include the impacts of intrusions to characterize their implications for large-scale circulation.

From a naval perspective, thermohaline intrusions are also of interest because of their effects on the performance of underwater sonar. A distinguishing feature of intrusions is their tendency to form characteristically sharp temperature and salinity interfaces that directly affect the sound-speed profile. The sharp density interfaces that arise from the alternating interleaving motions of intrusions lead to rapid changes in sound speed, which can distort or reflect acoustic signals. Navy operations rely heavily on acoustic propagation for underwater communication, detection of targets, targeting of adversaries, and underwater navigation. Intrusive layers can also trap and duct sound and alter the range of acoustic detection. The ducting effects of intrusions could potentially open possibilities for longer detection and communication ranges but, on the other hand, could also obstruct these processes by limiting the vertical propagation of sound waves. Such effects are particularly prominent for regions with a significant presence of intrusions, such as the Arctic, which is receiving more naval attention as the reduction of ice has opened more pathways for oceanic travelers and access to resources (Greenert 2014). A better understanding of thermohaline intrusions would therefore increase naval operational readiness by predicting such acoustic distortions.

B. BACKGROUND/LITERATURE REVIEW

To understand intrusions, it is important to address the physical mechanisms of their development. Intrusions are a double-diffusive phenomenon that develops in regions with vertical and horizontal gradients in temperature and salinity. They are characterized by horizontal interleaving with a small slope and derive from primary small-scale double-diffusive instabilities. These instabilities develop in fluids with two density-contributing components (often temperature and salinity) that diffuse at different rates. Stern (1960) first developed the theory of the double-diffusive fingering instability (or fingering convection); this process is most commonly found in the mid-latitude thermocline, characterized by steep temperature gradients. Fingering convection is a small-scale (few centimeter) process, but it has been shown to have large-scale implications in the ocean,

such as aiding the development of thermohaline intrusions (Stern 1967). The field has been reviewed extensively by Schmitt (1993), Schmitt (2004), and Radko (2013).

To consider the physical mechanism of intrusions, we present a simplified diagram of the relevant processes in Figure 1. The fluid is stratified vertically with warm and salty water above cool and fresh water. Isotherms and isohalines are sloped and shown by the dashed lines. Consider interleaving structures as shown in the figure, alternating in the direction of the flow and with slopes that are less inclined than the isotherms. Because temperature and salinity increase upward, salt fingers can develop at the fronts between these interleaving structures, indicated by the large arrows on the figure. Those traveling downward (D) are carrying cool and fresh water into warmer and saltier environments while those traveling upward (U) are carrying warm and salty water into cooler and fresher environments. This changes the local gradients across the fronts (A and B) between the interleaving structures. Front A is below the U structure and above the D structure. This means that the gradients are intensified (the warm water above is getting warmer, and the cool water below, cooler), which would suggest that the fingering fluxes should also increase. The opposite mechanisms happen at front B, which is below the D structure and above the U structure. At front B, the gradients become weaker (the warm water above is getting cooler and the cool water below, warmer), and the fluxes are consequently weaker. This means that there is a convergence in flux in the D structure and a divergence in flux in the U structure, as indicated by the size of the curved flux arrows in the figure. This results in the D structure becoming warmer and saltier and the U structure, cooler and fresher because of the influence of the salt fingers at the fronts. This effect can control the lateral transport of the interleaving structures. Because salt fingers transport salinity more effectively than temperature, this means that the downward traveling D structure can (depending on the slope of the intrusion and the strength of the fingering convection) become denser than its surroundings and therefore continue to descend (and vice versa for the upward traveling structure). Based on this behavior, the density perturbation of both upward and downward intrusions intensify due to salinity transport, which reinforces their original motions and promotes a positive feedback mechanism that causes intrusions to grow and sustain themselves (Radko 2013). Note that Figure 1 describes salt-finger-

induced intrusions, but other intrusion-favorable environments exist. For example, diffusive convection, characterized by negative gradients of temperature and salinity, would instead generate positively sloped interleaving structures.

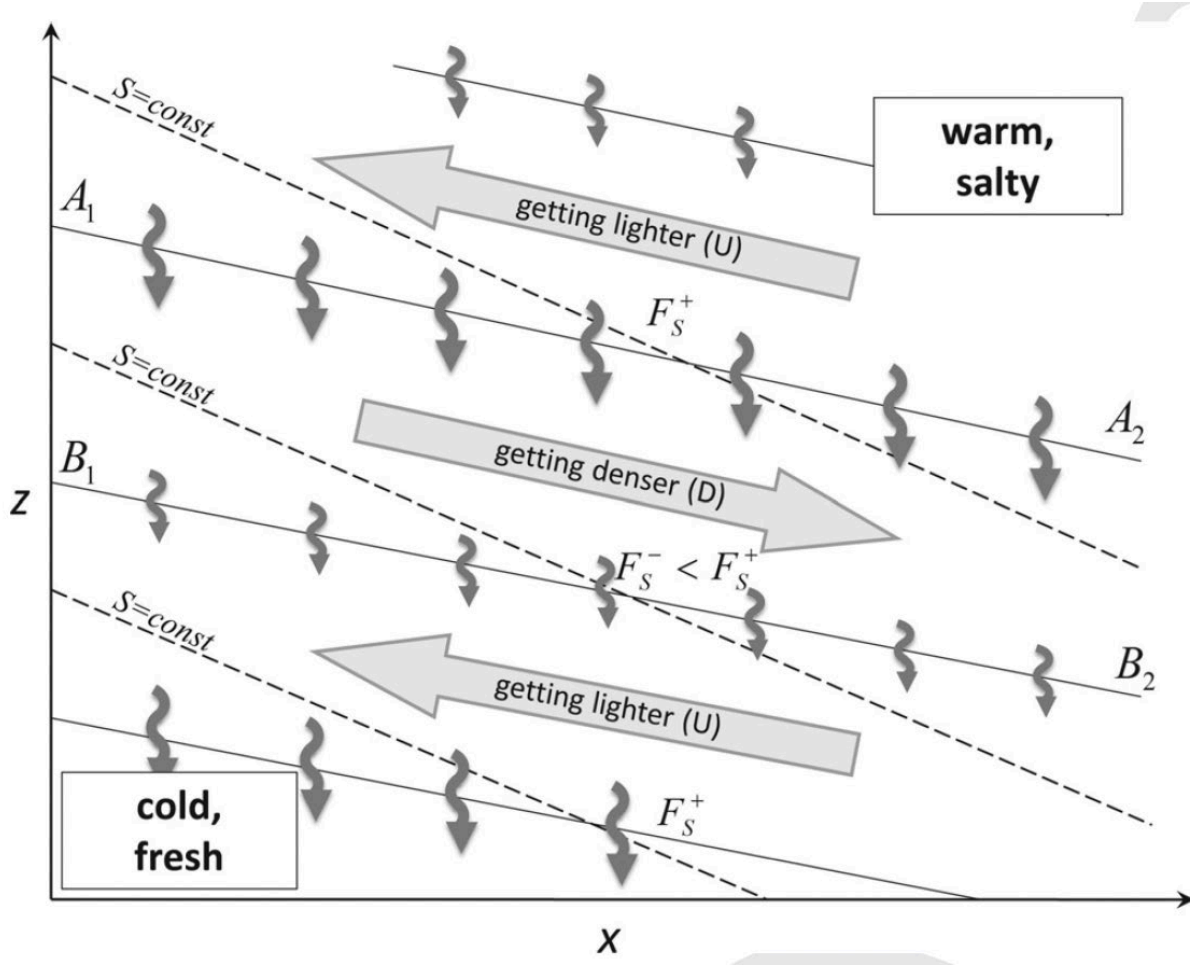

Figure 1. The physical mechanism of thermohaline interleaving.
Source: Radko (2013).

Another case that is similar to salt-finger-induced intrusions is the collective instability (also discovered by Stern 1969), which is an oscillating instability that develops due to the collective behaviors of salt fingers. Consider the same setup of Figure 1 but with the interleaving structures sloped the other way. In this case, downward traveling structures become warmer and saltier than their surroundings, the opposite as in the case of intrusions.

This reverses the convergence and divergence of flux described above, which results in downward traveling structures becoming lighter than their surroundings. Ordinarily, this setup would produce internal waves that propagate through the domain, but in this case, the additional flux convergence makes the oscillations over-stable.

Much of the literature about intrusions has focused on the salt-finger-driven case due to its prevalence in the thermocline of the ocean at the mid-latitudes. Intrusion characteristics were first studied in laboratories (Turner and Chen 1974), where intrusions, for technical reasons, where created using sugar and salt as diffusing substances. In the late 1970s intrusions were discovered in the Drake Passage (Joyce et al. 1978). Joyce et al. (1978) found that double-diffusive intrusions have characteristic vertical scales of 50–100m and very long horizontal scales. Joyce et al. (1978) estimated the lateral fluxes from their data using measurements of the local dissipation rates and found that such fluxes could have large-scale implications to the balance of heat and salt transfer in the Southern Ocean. Turner (1978) studied the double-diffusive mixing and transport across intrusion fronts by creating a sugar-salt laboratory experiment. Turner concluded that the opposing gradients of salt and sugar produced strong rapid spreading in all directions and generated substantial shear. The horizontal inclinations of these structures nearly align with the isotherms, which was shown in Ruddick and Turner (1979), and the dependence on horizontal gradients was further explored by Holyer (1983). However, the effects of external processes on these inclinations are generally uncharacterized (Radko 2013). Early analytic models used a constant eddy diffusivity, such as Toole and Georgi (1981), but it was not until the mid-1990s that a variable eddy diffusivity (as a function of density ratio) was used in such models, such as in Walsh and Ruddick (1995), Merryfield (2000), and in Smyth and Ruddick (2010). Many studies have focused on the role of microscale mixing processes and intrusions on large-scale circulation (e.g., Merryfield 2005; Garrett 1982). A numerical study by Radko and Sisti (2017) confirmed that intrusions are an ultimate cause of dispersion of Meddies intra-thermocline vortices of Mediterranean origin.

As high-performance computing has become more prevalent, numerical simulations have become a powerful tool in the study of intrusions and other microscale processes. However, fully resolved simulations of intrusions are impractical at present due

to the resolution requirements of these processes: the horizontal scale of the intrusions, 1km, exceeds the scale of the mixing that drives these structures, 1cm, by five orders of magnitude. Past research has used additional assumptions to compensate for these domain requirements in multi-dimension models. For example, Simeonov and Stern (2007) developed a two-dimensional fully resolved simulation using the prescribed tilt for the intrusions from the linear results of Toole and Georgi (1981), which estimated the inclination of the most unstable linear mode in the system. These fully resolved simulations evolved to an equilibrium state containing both salt-finger and diffusive interfaces, bounded by well-mixed layers. Their results suggest that the vertical salinity fluxes from intrusions are a factor of two larger than undisturbed fingers (Simeonov and Stern 2007). They also highlighted that a larger domain is needed in order to allow for slower growth rates of longer wavelength to develop.

There have also been a handful of studies that have investigated the generation of intrusions through single-dimensional parametric models (Mueller et al. 2007; Walsh and Ruddick 1998; Merryfield 2000). These models assume that the mixing caused by microstructure, shear, and convection can all be modeled as functions of local properties, which permits simulations without the need to resolve the dissipative scales. Walsh and Ruddick (1998) found that the inversions of salinity and temperature stabilize the intrusions into an equilibrium state as salt fingering and diffusive convection take over. Mueller et al. (2007) expanded the study of Walsh and Ruddick (1998) to include the effects of shear and convective turbulence on the development of intrusions. They found that the inclusion of these processes substantially reduced the horizontal fluxes. Finally, Merryfield (2000) showed that some intrusions could develop into double-diffusive staircases, the origins of which remain under debate in places such as the Arctic.

In this study, we perform fully resolved simulations to better understand the development of intrusions. We find that the mixing caused by intrusions is primarily caused by meter-scale processes such as convection and shear. It is identified that prior salt-finger models (constructed in the absence of large-scale flows) overpredict the transport of the microstructure fluxes of fingers within intrusions by a factor of two. We demonstrate that meter-scale shear serves as a critical component to the lateral transport of salt and

temperature in the system. We show that this mixing is not well represented by one-dimensional models.

This thesis is structured as follows. Chapter II discusses the setup for our fully resolved simulations, including the governing equations, scales, and nondimensional expressions, and our general model details. Chapter III outlines the results of our fully resolved simulations and compares, evaluates, and discusses our simulated models against previous empirical and analytical expressions for the mixing of relevant microscale processes. Chapter IV discusses the parameterized model setup and results. Finally, Chapter V provides conclusions and recommendations for future work.

THIS PAGE INTENTIONALLY LEFT BLANK

II. DIRECT NUMERICAL SIMULATIONS METHODOLOGY

This thesis explores double-diffusive intrusions through fully resolved numerical simulations. In this section, we discuss the governing equations, model assumptions, and the primary parameters of our numerical simulations. This work uses Direct Numerical Simulations (DNS) which evolve the fluid governing at the full range of spatial scales, including the viscous, thermal, and haline dissipation scales. DNS are used in many fields to simulate and study processes of fluid dynamical interest where the small-scale mixing features are important. In our study, we utilize DNS to directly model the smallest mixing scales found in intrusions to compare the fluxes of the microscale processes to analytical prescriptions.

For our multi-dimensional DNS of intrusive systems, we use nondimensional versions of the governing equations for a two-component Boussinesq system in the absence of external forcing or rotation (Pedlosky 1979). The full set of dimensional governing equations are given by

$$\frac{\partial T^*}{\partial t^*} + \vec{v}^* \cdot \nabla^* T^* = k_T \nabla^{*2} T^*, \tag{1}$$

$$\frac{\partial S^*}{\partial t^*} + \vec{v}^* \cdot \nabla^* S^* = k_S \nabla^{*2} S^*, \tag{2}$$

$$\frac{\partial \vec{v}^*}{\partial t} + \vec{v}^* \cdot \nabla^* \vec{v}^* = -\frac{\nabla p^*}{\rho_0} + g\frac{\rho - \rho_0}{\rho_0} + \nu \nabla^{*2} \vec{v}^*, \tag{3}$$

$$\nabla^* \cdot \vec{v}^* = 0, \tag{4}$$

where ν is the kinematic viscosity, k_T is the thermal diffusivity, k_S is the salinity diffusivity, g is the acceleration due to gravity constant, $\vec{v}^*$ is the velocity, p^* is the local pressure, ρ^* is the local density, T^* is the local temperature, S^* is the local salinity, and ρ_0 is a reference density. The asterisks indicate that the variable is dimensional. The Boussinesq approximation posits that the density perturbation is well approximated by a linear function of temperature and salinity, as

$$\frac{\rho^* - \rho_0}{\rho_0} = \beta(S^* - S_0) - \alpha(T^* - T_0), \tag{5}$$

where the constant coefficients α and β are the thermal expansion coefficient and haline contraction coefficient of the seawater, respectively. The parameters S_0 and T_0 are the reference values for ocean salinity and temperature, respectively. We define the thermal and salinity perturbations away from a constant gradient as $T' = T^* - {T_0}^* - {\bar{T}_z}^* z^* - {\bar{T}_x}^* x^*$, where ${\bar{T}_x}^*$ is the background vertical thermal gradient and ${\bar{T}_x}^*$ is the background horizontal thermal gradient, and $S' = S^* - {S_0}^* - {\bar{S}_z}^* z^* - {\bar{S}_x}^* x^*$, where ${\bar{S}_z}^*$ is the background vertical salinity gradient and ${\bar{S}_x}^*$ is the background horizontal salinity gradient.

In order to express the governing equations non-dimensionally, we establish a non-dimensional scale for each of the dimensional variables. The non-dimensional length scale used is *d*, which is given by

$$d = \left(\frac{k_T \nu}{g\alpha|\bar{T}_z|}\right)^{\frac{1}{4}}. \tag{6}$$

In the ocean thermocline, *d* is typically 1cm. The remaining non-dimensional scales are chosen to be consistent with the broader double-diffusive literature: they are explained in detail in Radko (2013) and listed in Table 1. The non-dimensional equations are then given by

$$\frac{1}{Pr}\left(\frac{\partial \vec{v}}{\partial t} + \vec{v} \cdot \nabla \vec{v}\right) = -\nabla p + (T' - S')\vec{k} + \nabla^2 \vec{v}\,, \tag{7}$$

$$\frac{\partial T'}{\partial t} + \vec{v} \cdot \nabla T' + w + Gu = \nabla^2 T'\,, \tag{8}$$

$$\frac{\partial S'}{\partial t} + \vec{v} \cdot \nabla S' + \frac{w}{R_\rho} + Gu = \tau \nabla^2 S'\,, \tag{9}$$

$$\nabla \cdot \vec{v} = 0\,, \tag{10}$$

where τ is the diffusivity ratio, $\tau = \frac{\kappa_S}{\kappa_T}$; Pr is the Prandtl number, $\mathrm{Pr} = \frac{\nu}{\kappa_T}$; *G* is the non-dimensional lateral gradient of temperature and salinity; and R_ρ is the density ratio, $R_\rho =$

$\frac{\alpha\bar{T}_z}{\beta\bar{S}_z}$. In constructing these equations, we are considering only the situation where $\bar{T}_z > 0$and $\bar{S}_z > 0$, which is typical of the mid-latitude thermocline. The lateral gradients of temperature and salinity must exactly match in this non-dimensionalization to keep the density field horizontally uniform.

Table 1. Nondimensional variable scales.

Scales	Expression	Ocean values
Time	$\langle t \rangle = \frac{d^2}{k_T}$	10^3 s
Length	$\langle L \rangle = d$	0.01 m
Velocity	$\langle v' \rangle = \frac{k_T}{d}$	10^{-5} m s^{-1}
Temperature perturbation	$\langle T' \rangle = d\lvert\bar{T}_z\rvert$	10^{-4} ºC
Salinity perturbation	$\langle S' \rangle = \frac{\alpha}{\beta}\langle T' \rangle$	2.7×10^{-5}psu
Density perturbation	$\langle \rho \rangle = \rho_0$	1000kg/m^3
Pressure perturbation	$\langle p' \rangle = \frac{\rho_0 \upsilon k_T}{d^2}$	1.4×10^{-6} Pa

We evolve these equations using the numerical code PADDI (Traxler et al., 2011), which has been used historically to handle a wide variety of double-diffusive problems. This code is pseudo-spectral and uses the Patterson-Orzag method (Canuto et al. 2007) to enforce incompressibility. It evolves the equations over time using a third-order semi-implicit Adams–Bashforth/Backward-Difference Formula (Peyret 2002), which provides sufficient accuracy for this work. The diffusive terms are treated implicitly, whereas the remaining terms are treated explicitly. This allows the time-steps to be limited by the Courant time scale rather than a diffusive time scale. (Traxler et al. 2011). PADDI is

designed to run efficiently on massively parallel supercomputers and employs a transpose-based parallel transform algorithm (Stellmach and Hansen 2008). The code decomposes the perturbation fields into Fourier modes and is periodic in all directions, a convention which was first introduced to double-diffusive studies by Shen (1995).

The primary parameters that govern these simulations are the density ratio, the horizontal gradients, and the size of the domain. We simulate three density ratios for the simulations, $R_\rho = (1.5,2,3)$, which are selected as they span commonly observed values in the thermocline of the ocean. In addition, linear stability analysis shows that the strongest growing intrusive modes occur below a density ratio of three (Radko 2011), so this work also adequately characterizes the most dynamically important region of parameter space. Each of the density ratios is simulated in three two-dimensional domains with varying domain sizes: 5000 by 500, 2500 by 500 and 500 by 500 with aspect ratios of A=10, A=5 and A=1, respectively. Typical values of G in the ocean are around 0.001, but this results in an intrusive aspect ratio much larger than will fit in the domain. In our numerical simulations, we therefore set the gradient to 0.1 for these numerical constraints.

III. DNS RESULTS

A. FLOW-FIELD EVOLUTION

We begin by demonstrating the characteristic behavior of our intrusion simulations in Figure 2. We show the salinity perturbation field of a simulation with a density ratio of 2, horizontal gradient of 0.1 and aspect ratio of 10 at times $t = 91$, $t = 302$ and $t = 412$. This figure displays the development of alternating bands of salty fluid that oscillate in time in Figure 2c. These structures arise from inclined flows that alternate vertically and horizontally. Low-salinity material travels from the bottom right to the top left, adjacent to high-salinity material traveling in the opposite direction. Salt fingers can easily be seen between these regions, and these salt fingers drive the intrusions. Two different solutions are expected, as described in Radko (2013): oscillating collective instability modes and direct intrusive modes. Both of these processes can be explained using mean-field analysis based on parametric models of microstructure (see Chapter IV). Figure 2b,c shows an example of the former as these structures oscillate in time and are inclined in the opposite direction as the isotherms. Note that this does not preclude the possibility of the direct intrusive mode (which typically grows more slowly) forming at later times, though such behavior is not seen here. Because of the fine resolution of this simulation, the salt-fingers between the intrusions are fully resolved, as shown in Figure 2d. The temperature perturbation field is shown in Figure 3 for t=412, and it appears morphologically similar to the salinity perturbation field.

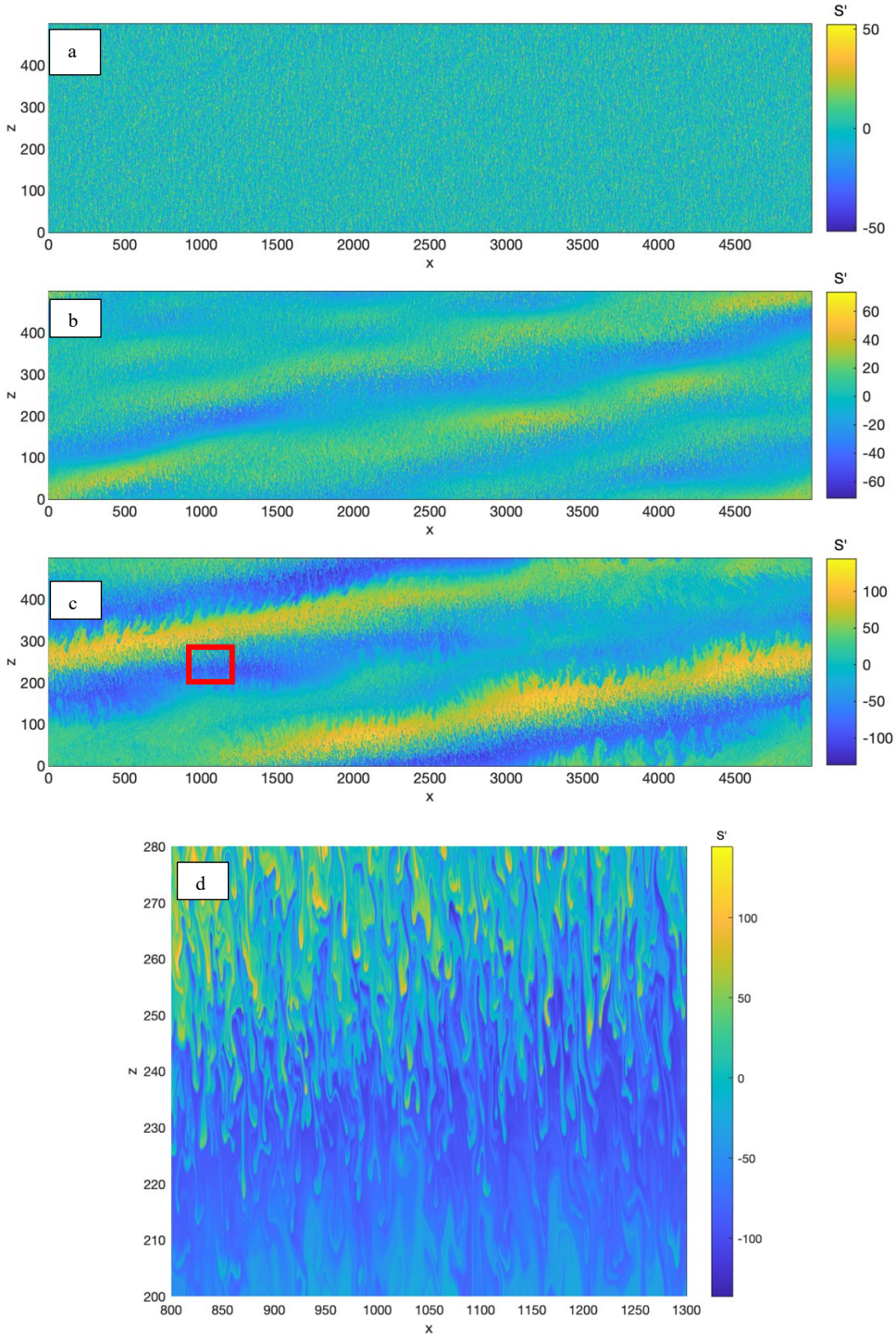

Figure 2. Salinity perturbations in DNS (x–z plane).

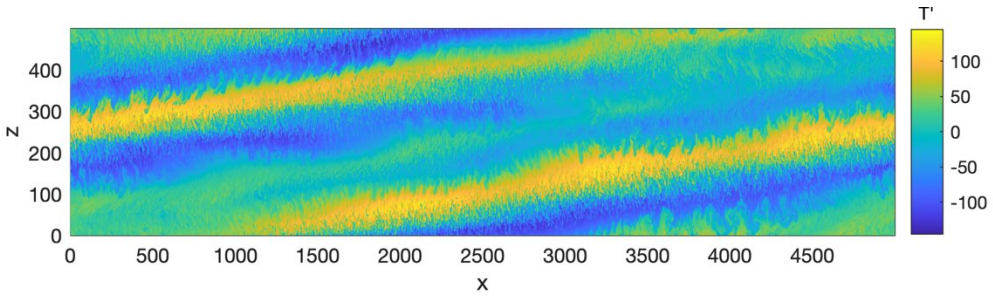

Figure 3. Temperature perturbation in DNS (x–z plane).

Figure 3 displays the temperature perturbation in the same x-z frame as Figure 2. The differences between the temperature perturbation and salinity perturbation fields are minimal since they are proportional to each other. Figure 3 also seems hazier due to the temperature diffusing quicker than the salinity.

Figure 4 displays the evolution of the vertical haline and vertical thermal fluxes for simulations with density ratios of 1.5, 2, and 3, an aspect ratio of 10, and a gradient of 0.1. The vertical fluxes of temperature and salinity are defined as

$$F_T = \langle wT' \rangle, \tag{11}$$

$$F_S = \langle wS' \rangle, \tag{12}$$

where angled brackets indicate the average over the entire simulated domain. The thermal (top) and haline fluxes (bottom) grow exponentially until t = 91. This occurs because, at early times, the perturbations to the fields are small, as shown in Figure 2a, and the governing equations are well-approximated by their linear forms, the solutions to which are exponential. As the salt-finger perturbations grow, the nonlinear terms become important and the system reaches a quasi-statistical equilibrium. These saturated fingers transport both temperature and salinity downward. Based on Figure 4, we compare the buoyancy fluxes of temperature and salinity, which are equivalent to F_T and F_S in our non-dimensionalization, using the flux ratio, γ. We define the flux ratio as

$$\gamma = \frac{F_T}{F_S}, \tag{13}$$

which is typically around 0.5–0.7 for double-diffusive processes. This is consistent with our results. The lower value of the buoyancy flux due to temperature results from temperature diffusing more efficiently into surrounding fluid than salinity, which leads to turbulent motion transporting salinity more effectively. This behavior is consistent across all values of the density ratio explored in this study.

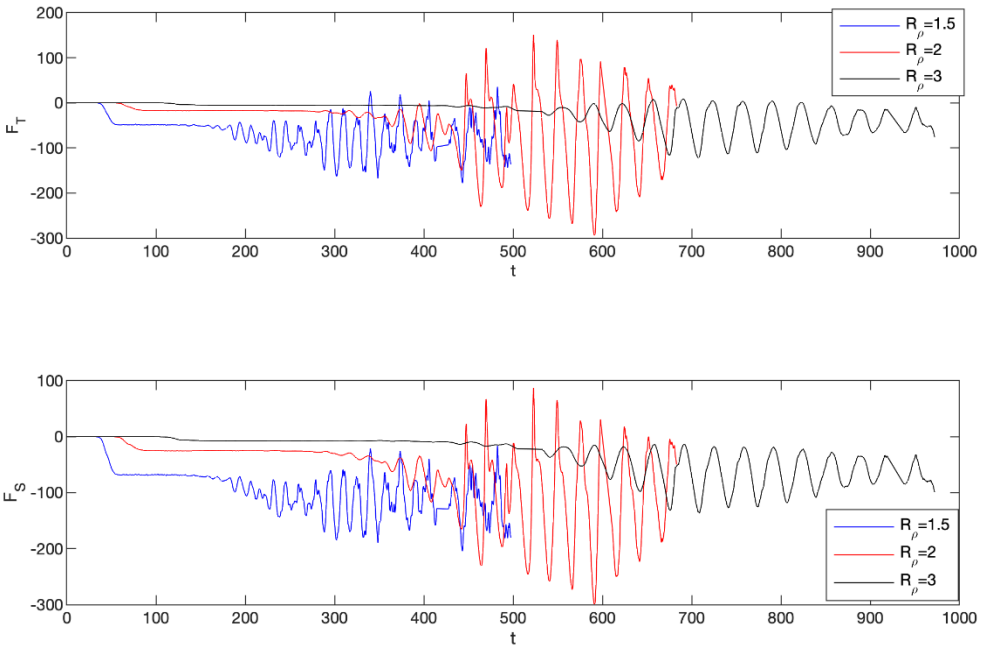

Figure 4. Time-series of vertical fluxes in DNS for three different density ratios.

Figure 5 shows the horizontal fluxes for the same simulations. The horizontal fluxes of temperature and salinity are defined as

$$F_{T,H} = \langle uT' \rangle, \tag{14}$$

$$F_{S,H} = \langle uS' \rangle. \tag{15}$$

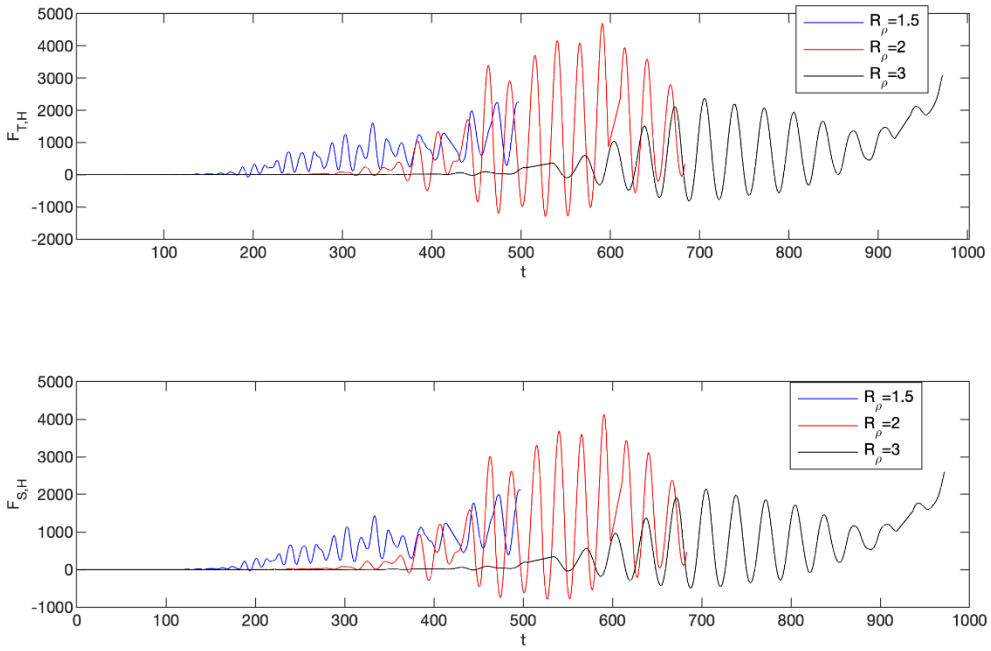

Figure 5. DNS horizontal fluxes as a function of time.

The horizontal fluxes are negligible at early times until t=100, at which point they gradually begin to amplify. Once the collective instability becomes dynamically significant around t=300, the interleaving structures begin to transport material laterally. This change arises because the horizontal transport of isolated salt fingers is typically negligible, but as large-scale shear becomes more prevalent through the collective instability, the vertical mixing can translate to horizontal transport. We also note that the horizontal fluxes become much larger than the vertical fluxes when the large-scale processes become prominent. This is due to the large horizontal component of the velocity in these structures, which are only slightly inclined. This can be seen in Table 2 where the time averages, denoted with an overbar, of the temperature and salinity fluxes from the DNS are recorded. Generally, the horizontal fluxes are larger by a factor of 8 in these simulations than the vertical fluxes. However, the fluxes noticeably decrease as the density ratio increases.

Table 2. Averaged fluxes for each DNS.

Density Ratio R_ρ	Aspect Ratio A	Vertical $\overline{F_T}$	Vertical $\overline{F_S}$.	Horizontal $\overline{F_{T,H}}$.	Horizontal $\overline{F_{S,H}}$.
1.5	10	-77.05	-111.2	748.1	725.3
2	10	-61.11	-90.54	967.4	962.1
3	10	-36.14	-52.65	698.7	675.4
1.5	5	-125.6	-189.8	1666	1686
2	5	-68.99	-126.0	2100	1919
3	5	-66.30	-136.0	3064	2790
1.5	1	-719.0	-434.9	6635	6681
2	1	-422.0	-600.6	4580	4681
3	1	-281.5	-526.3	5367	5394

Figure 6 displays the averaged haline and thermal fluxes as functions of density ratio for all aspect ratios. Radko and Smith (2012) found that fluxes decrease with increasing density ratio, which is consistent with our results. As the density ratio increases, both the haline and thermal fluxes decrease, which is consistent with the general literature of salt fingers. This shows that the aspect ratio of 10 works for all three density ratio simulations because both the horizontal and vertical fluxes do not vary much from the A = 5 cases. That said, the aspect ratio of 1 case differs from the other two aspect ratios because they develop into thermohaline staircases, which is confirmed by the visual inspection of the simulations. Another tell-tale sign of the formation of thermohaline staircases, fluxes sharply increase before they equilibrate with a new average value. This observation also agrees with previous studies (Radko 2003; Merryfield 2000), which show that systems with low density ratios (R_ρ =1.7 and below), tends to form thermohaline staircases by the gamma-instability. The gamma-instability only occurs when γ decreases

as a function of the density ratio. This instability amplifies density perturbations (making dense regions denser and vice versa), which results in the formation of thermohaline staircases, which typically have more extreme fluxes. Schmitt (1979) was the first to give an estimate for the minimum value of the flux ratio (i.e., the upper limit for which staircases would be expected), finding it around a density ratio of 4. A later study by Traxler et al. (2011) determined it to instead be approximately 7 through numerical experiments. Therefore, thermohaline staircases are theoretically possible in any of our simulations.

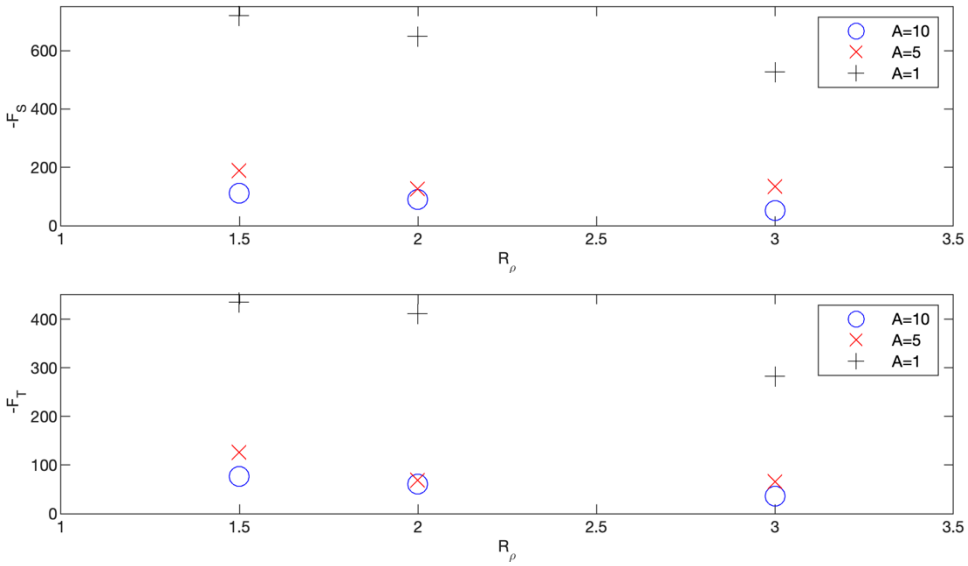

Figure 6. DNS averaged fluxes for different density ratios.

B. MODEL COMPARISON

In this section, we will examine each individual mixing process against existing models to determine how well such models perform within the turbulent intrusion environment. Typically, microstructure mixing models are constructed under the assumption that the environment is quiescent, but such is rarely the case in nature. We can address this assumption by removing the fluxes of large-scale flows. To do so, we determine the local perturbations of velocity, temperature, and salinity. This is achieved by first smoothing the $\vec{v}$, S', and T' fields by removing Fourier modes with wavelengths smaller than some cutoff scale, c. This creates smoothed versions of the fields v^{sm}, S^{sm},

and T^{sm}. Then, we generate the perturbations away from those smoothed profiles by, $v'' = v' - v^{\mathrm{sm}}$, $S'' = S' - S^{\mathrm{sm}}$, and $T'' = T' - T^{\mathrm{sm}}$. We decompose the domain into squares of length $l = 0.01$ and then evaluate the turbulent fluxes at scale l by taking the local mean of the vertical fluxes and gradients, i.e., $\langle w''T'' \rangle_l, \langle w''S'' \rangle_l$, $\langle \frac{dS}{dz} \rangle_l$, and $\langle \frac{dT}{dz} \rangle_l$. We then construct the effective haline diffusivity as

$$K_S = -\frac{\langle w''S'' \rangle_l - \langle \frac{\partial S}{\partial z} \rangle_l}{\langle \frac{\partial S}{\partial z} \rangle_l}, \tag{16}$$

the effective thermal diffusivity as

$$K_T = -\frac{\langle w''T'' \rangle_l - \langle \frac{\partial T}{\partial z} \rangle_l}{\langle \frac{\partial T}{\partial z} \rangle_l}. \tag{17}$$

This is done for each square and at temporal intervals of 5 to yield a large sample of instances of various small-scale processes. We identify them in terms of the local vertical gradients of temperature and salinity, the density ratio, $R_{\rho l} = \langle \frac{\partial T}{\partial z} \rangle_l \,/\, \langle \frac{\partial S}{\partial z} \rangle_l$, the Richardson number, $Ri_l = Pr \left(\langle \frac{\partial T}{\partial z} \rangle_l - \langle \frac{\partial S}{\partial z} \rangle_l \right) / \langle \frac{\partial u}{\partial z} \rangle_l^2$, and the Rayleigh number, $Ra_l = \left(\langle \frac{\partial S}{\partial z} \rangle_l - \langle \frac{\partial T}{\partial z} \rangle_l \right) H_l^4$, where H_l is the total height of any local convection region defined by the region where $\bar{S}_z + \langle \frac{\partial S^{\mathrm{sm}}}{\partial z} \rangle_l - \bar{T}_z - \langle \frac{\partial T^{\mathrm{sm}}}{\partial z} \rangle_l > 0$. We define a region of salt-fingering to exist where $\bar{T}_z + \langle \frac{\partial T^{\mathrm{sm}}}{\partial z} \rangle_l > 0$ and $1 < R_{\rho l} < 100$, a region of diffusive convection where $\bar{T}_z + \langle \frac{\partial T^{\mathrm{sm}}}{\partial z} \rangle_l < 0$ and $0 < R_{\rho l} < 1$, and a region of convection where $\mathrm{Ra}_l > 1000$. These three identifications are exclusive. We also define a shear-dominated region anywhere that $0 < Ri_l < 1$, which is exclusive to the convection region but can coexist with double-diffusive convection. Regions with more than one relevant process (e.g., fingering convection in the presence of shear) are ignored in this discussion.

The values of K_S derived from the simulation with density ratio 2 and aspect ratio 10 are shown in Figure 7, categorized by process and plotted against the relevant governing parameter (density ratio for double-diffusive processes, Richardson number for shear, and

Rayleigh number for convection). This allows us to determine whether the models of the microstructure processes that were generated in quiescent environments still apply in the turbulent environment of intrusions. We see that each of the microscale processes outlined above are present in the intrusions. As with many microscale processes, the effective diffusivities of temperature and salinity are comparable as both are advected by turbulent motion. For this reason, we focus our discussion on the effective haline diffusivity.

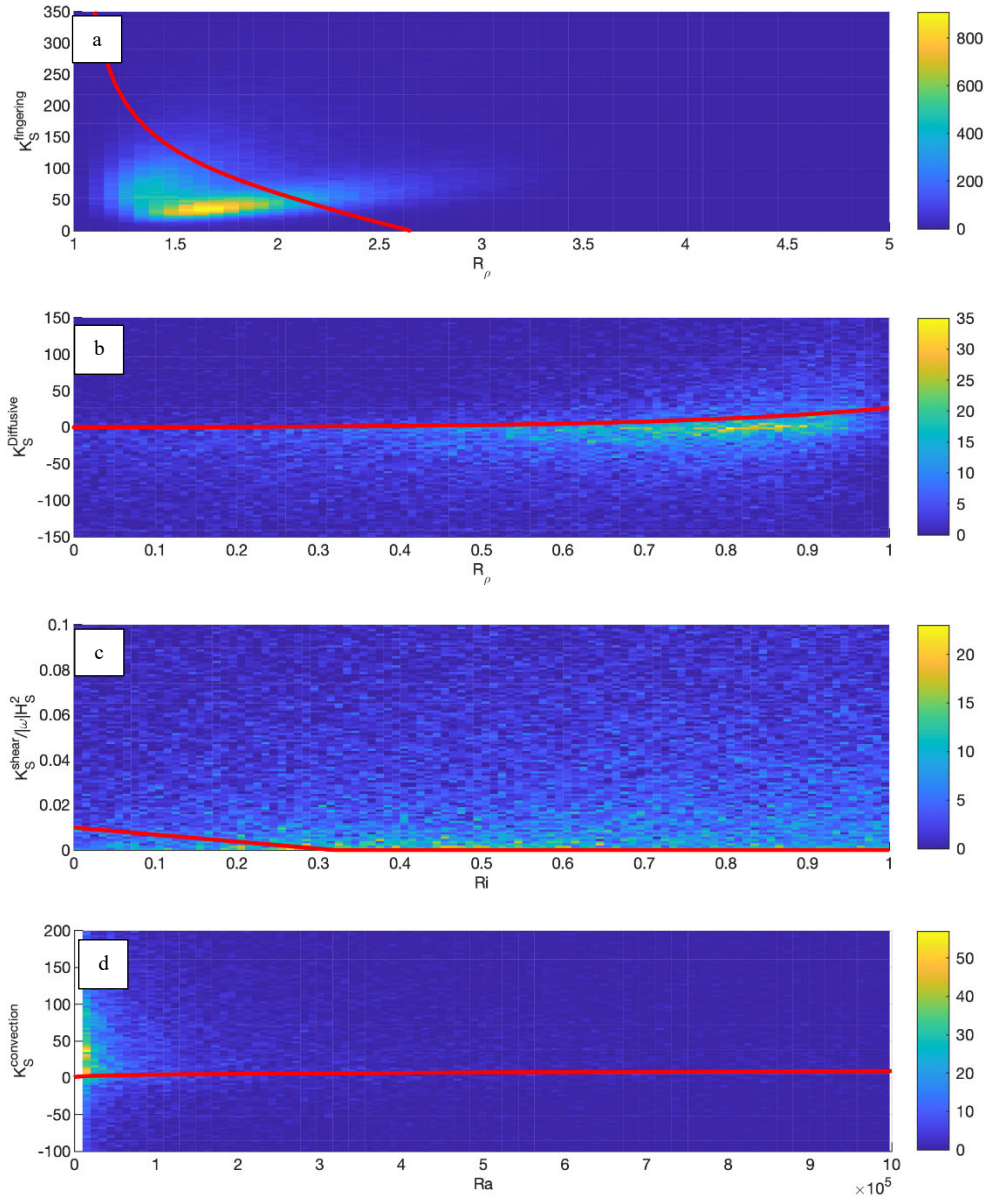

Figure 7. Density plots of DNS small-scale mixing regimes.

In Figure 7a, we compare measurements of K_S in salt-fingering regions from our simulation with an analytical model from Radko and Smith (2012) and Radko (2014). The predicted salt-finger diffusivity model from Radko and Smith (2012) takes the following form

$$K_s{}^{fingering} = \left(\frac{a_s}{\sqrt{(R_{\rho l} - 1)}} + b_s \right) R_{\rho l}, \tag{18}$$

$$\gamma^{fingering} = a_\gamma exp\left(-b_\gamma R_\rho\right) + c_\gamma, \tag{19}$$

where a_s, b_s, a_γ, b_γ, and c_γ are constant coefficients fitted to numerical simulations to yield values of 136.9, -105.13, 4.752, -3.318, and 0.59, respectively, for two-dimensional simulations. The molecular diffusivity of salinity from the model is represented by $K_s{}^{\text{fingering}}$. The implications of this model choice for use in a larger parametric model will be discussed in Chapter IV. The effective diffusivity measured from the simulations behaves comparably to the Radko and Smith (2012) and Radko (2014) models at low density ratio. Figure 7a shows that the effective diffusivity measured from the simulations does not compare well with the model. The model overpredicts the salinity diffusivity for a given local density ratio by a factor of 2.7 around a density ratio of 1.7. As the local density ratio increases, there are fewer instances of salt fingering, but the fluxes tend to increase. This may suggest that other forms of microscale mixing are more prevalent in our simulation at such density ratios.

In Figure 7b, we plot the Kelly (1990) model alongside the local calculations of the effective diffusivities to analyze the mixing caused by diffusive convection. This model is commonly used to represent the mixing by diffusive convection in the literature and is expressed as

$$K_s{}^{diffusive} = \gamma^{diffusive} C (Ra^{diffusive})^{\frac{1}{3}} \tag{20}$$

where $\gamma^{\text{diffusive}}$, C, and $\text{Ra}^{\text{diffusive}}$ are given by the following expressions:

$$\gamma^{diffusive} = \frac{R_\rho^{-1} + 1.4(R_{\rho l}^{-1} - 1)^{3/2}}{1 + 14(R_{\rho l}^{-1} - 1)^{3/2}}, \tag{21}$$

$$C = 0.0032exp\,[4.8(R_{\rho l}^{-1})^{0.72}], \tag{22}$$

$$Ra^{diffusive} = 0.25 \times 10^9 R_{\rho l}^{1.1}\,. \tag{23}$$

These prescriptions do not account for the effects of shear mixing. Figure 7b shows that the effective diffusivity for diffusive convection measured from the simulations compares well with the model trend at large density ratios, overpredicting our salinity diffusivity slightly. At lower density ratios, most of the instances of diffusive convection in the simulation appear to be anti-diffusive. This suggests that other processes are involved or that the relevant gradients are too small to produce meaningful effective diffusivities.

In addition, in Figure 7c, we plot the local calculations of the effective diffusivities from the simulation to compare with a shear mixing model adapted from Pope (2000). The model gives the expression for shear-driven mixing as $K^{\text{shear}} = a_0 H_s^2 |\omega|$ in the absence of external forcing when shear mixing is expected to dominate (i.e., $\text{Ri}_l < \text{Ri}_c$, where Ri_c is the critical Richardson number for dynamical instability and is typically taken to be near ¼). To create a continuous model, some studies (e.g., Ellison and Turner 1959; Xu et al. 2006) connected the shear-dominated regime to the dynamically stable regime with a linear piece-wise function as

$$K_S^{shear} = a_0 H_s^2 |\omega| \begin{cases} 1 & Ri_l < 0, \\ 1 - \frac{Ri}{Ri_c} & 0 \geq Ri_l \leq Ri_c, \\ 0 & Ri_l > 0, \end{cases} \tag{24}$$

$$\gamma^{\text{shear}} = 1,$$

where a_0 is a constant value set to 0.01. This value agrees well with experiments by Bell and Mehta (1990) and Rogers and Moser (1994). The vertical thickness of the sheared layer is represented by H_s, and the local magnitude of shear by ω. We determine H_s locally using the expression $\frac{\langle u \rangle_l}{\langle \frac{du}{dz} \rangle_l}$. The critical Richardson number, Ri_c, is set to 0.32 to ensure that all

turbulence is accounted for within the model. The model depends on three locally varying quantities, so we scale the plotted quantity as $\frac{K_S^{shear}}{H_S^2|\omega|}$ to reduce the model to a curve in Figure 7c. Figure 7c shows that the effective diffusivity for shear turbulence measured from the simulations compares well with the model for Richardson number. Generally, the figure reveals that most instances of shear mixing tend to occur above the critical Richardson number, and most of such instances do not demonstrate substantial mixing. This suggests that shear mixing is not an important process at these scales.

Finally, we compare our results with a model for convective mixing that was calibrated by Linden (2000) in Figure 7d. The expression is given by the well-known 1/3-power law that relates the flux of convection to the Rayleigh number

$$K_S^{convection} = Nu_0 \times \begin{cases} 0 & Ra_l \leq 0 \\ Ra_l{}^{\frac{1}{3}} & Ra_l > 0 \end{cases} \tag{25}$$

$$\gamma^{\text{convection}} = 1,$$

where Nu_0 was calibrated to a constant value of 0.09. Figure 7d shows that there are few instances of convection at Rayleigh numbers where convective mixing would be substantial. Instead, the most prevalent such regions tend to be for low Rayleigh numbers, where the gradients are small and diffusive treatments of mixing fail.

IV. PARAMETERIZED MODEL

A. PARAMETERIZED MODEL METHODOLOGY

We use a parameterized model that incorporates analytic prescriptions of double-diffusive mixing to develop large-scale simulations of ocean environments. These simulations allow for the investigation of the dynamic effects of microstructure on large-scale systems by expanding the parameter space of our simulations to include more realistic isothermal slopes than are possible with fully resolved models

The parameterized model is constructed using the PADDI framework by adapting the Boussinesq equations, Equations 7 through 10, with additional thermal and haline flux terms. We construct the parameterized Boussinesq equations, as

$$\frac{\partial T'}{\partial t} + Gu' + w' = \nabla \cdot K_T \nabla T', \tag{26}$$

$$\frac{\partial S'}{\partial t} + Gu' + \frac{w'}{R_\rho} = \nabla \cdot K_S \nabla S', \tag{27}$$

$$\frac{1}{Pr}\frac{\partial}{\partial t}\vec{v}' = -\nabla p' + (T' - S')\vec{k} + \nabla^2 \vec{v}', \tag{28}$$

$$\nabla \cdot \vec{v}' = 0, \tag{29}$$

where K_T and K_S are the parameterized thermal and haline diffusivities generated by the microstructure fluxes, which depend on the local properties of the flow. In the parameterized model, the diffusivity, K_S, is a function of the local density ratio and of local gradients of temperature and salinity. The effective haline diffusivity is given by

$$K_S = \begin{cases} K_S^{fingering}, \frac{\partial T}{\partial z} > 0 \; and \; 1 < R_{\rho l} < 2.70, \\ K_S^{diffusive}, \frac{\partial T}{\partial z} < 0 \; and \; 0 < R_{\rho l} < 1, \\ \tau, otherwise, \end{cases} \tag{30}$$

where 2.70 is chosen as the limit for fingering convection as that is the value for which the model becomes negative. The effective thermal diffusivity is instead given by

$$K_T = R_{\rho l}^{-1} \begin{cases} \gamma^{fingering} K_S^{fingering}, \frac{\partial T}{\partial z} > 0 \; and \; 1 < R_{\rho l} < 2.70, \\ \gamma^{diffusive} K_S^{diffusive}, \frac{\partial T}{\partial z} < 0 \; and \; 0 < R_{\rho l} < 1, \\ 1, otherwise. \end{cases} \quad (31)$$

As was shown in Chapter III, the prescriptions for convection and shear do not adequately represent the behavior of the system at small scales. The majority of the mixing by such processes is expected to be at larger scales and, as such, do not require prescriptions.

B. VERIFICATION

We constructed a parameterized simulation with the same parameters as in the case shown in Figure 4 with the intent to determine the reliability of the parameterized model. Both simulations have a density ratio of 2, an aspect ratio of 10 (500 by 5000), and the horizontal temperature gradient of 0.1. When comparing the DNS to the parameterized model results, it is evident that microscale mixing has a substantial influence. This can be seen in the comparison of the vertical and horizontal fluxes of the two models, which are shown in Figure 8 and which differ substantially. The early fluxes are comparable between the two cases. However, as the large-scale motions develop at around *t*=350, the fluxes in DNS start to oscillate (due to the collective instability) while the parameterized model only exhibits direct intrusive modes. As with other cases, the temperature fluxes (not shown here) behave similarly to the salinity fluxes. The parameterized model salinity fluxes are smaller than the DNS fluxes by a factor of 4, vertically and horizontally. This seems to be common when comparing the two evolutionary scenarios (further discussed in Subsection C) of the parameterized model and explains why the DNS displays collective instability whereas the parameterized model evolves into intrusions with matching parameters.

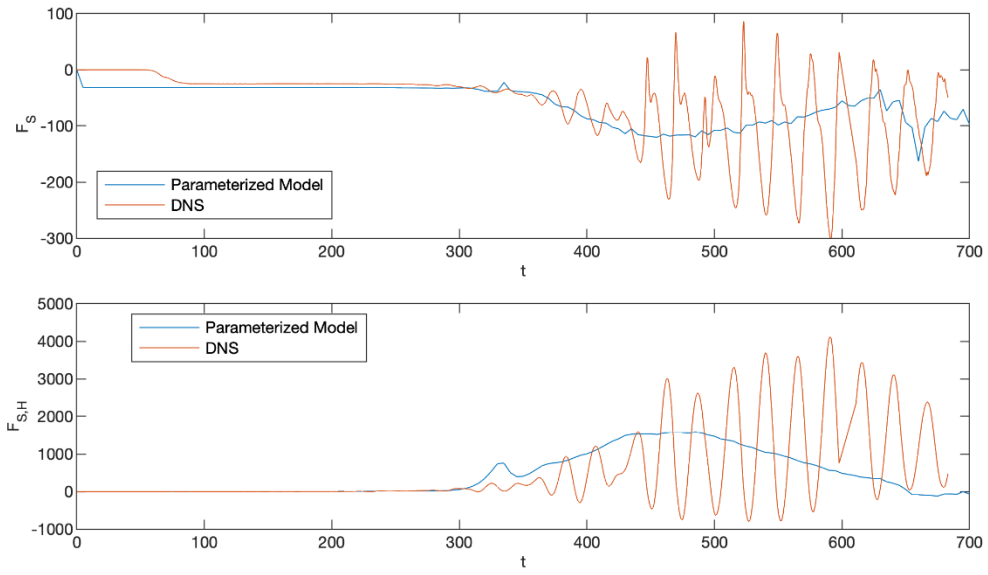

Figure 8. Comparison of the DNS and parameterized model fluxes.

C. PARAMETERIZED MODEL RESULTS

In our parameterized simulations, we vary the governing parameters R_ρ, A, and G to investigate the behavior of intrusions for parameters that are more oceanographically relevant. We run two simulations for each of the following gradients: 0.1, 0.03, 0.01, 0.001, 0.003. Each of the two simulations has an aspect ratio 10, but the domain of the boxes were 500 by 5000 and 4000 by 40000. In addition, for the gradient of 0.01, we also simulate an aspect ratio of 20 (4000 by 80000 domain) to ensure that the domain captures the full size of an intrusive mode. A density ratio of 2 is used for all simulated gradients and aspect ratios. For the gradient of 0.01, we simulate an additional two cases with density ratios of 2.5 and 3 to better understand the effects of the density ratio. We find that there are two types of evolutionary scenarios: the first scenario is characterized by the development of intrusions, which eventually merge into thermohaline staircases, and in the second scenario the flow field is dominated by persistent internal waves.

The first of these evolution scenarios is demonstrated in Figure 9, which displays the salinity perturbation field of the parameterized model with parameters of $R_\rho = 2$, A= 10, and G=0.1 at t=91, t=302, t=412, and t=1500 in the same manner as Figure 2. The

stratified field develops a mean-field analogy to diffusive convection (since the parameterized diffusivity of salinity exceeds that of temperature) in Figure 9a. As time progresses, direct intrusions begin to form in Figure 9b. By t=412 in Figure 9c, the vertical mixing in these structures has led to convective overturns in the interleaving regions. Comparing Figure 9a–c with Figure 2a–c, we see the development of inclined interleaving structures in both simulations. However, in Figure 2b, these structures are oscillating in time and inclined against the isotherms, whereas in Figure 9b, they are steady and inclined along the isotherms. These motions eventually generate inclined shear structures where dense material overlies lighter fluid and which then create thermohaline staircases, as shown in Figure 9d, where no inclined structures remain. This further suggests that although this parameterized model can reproduce qualitative features of systems with lateral gradients, its capacity to directly predict behavior of a given physical system is limited.

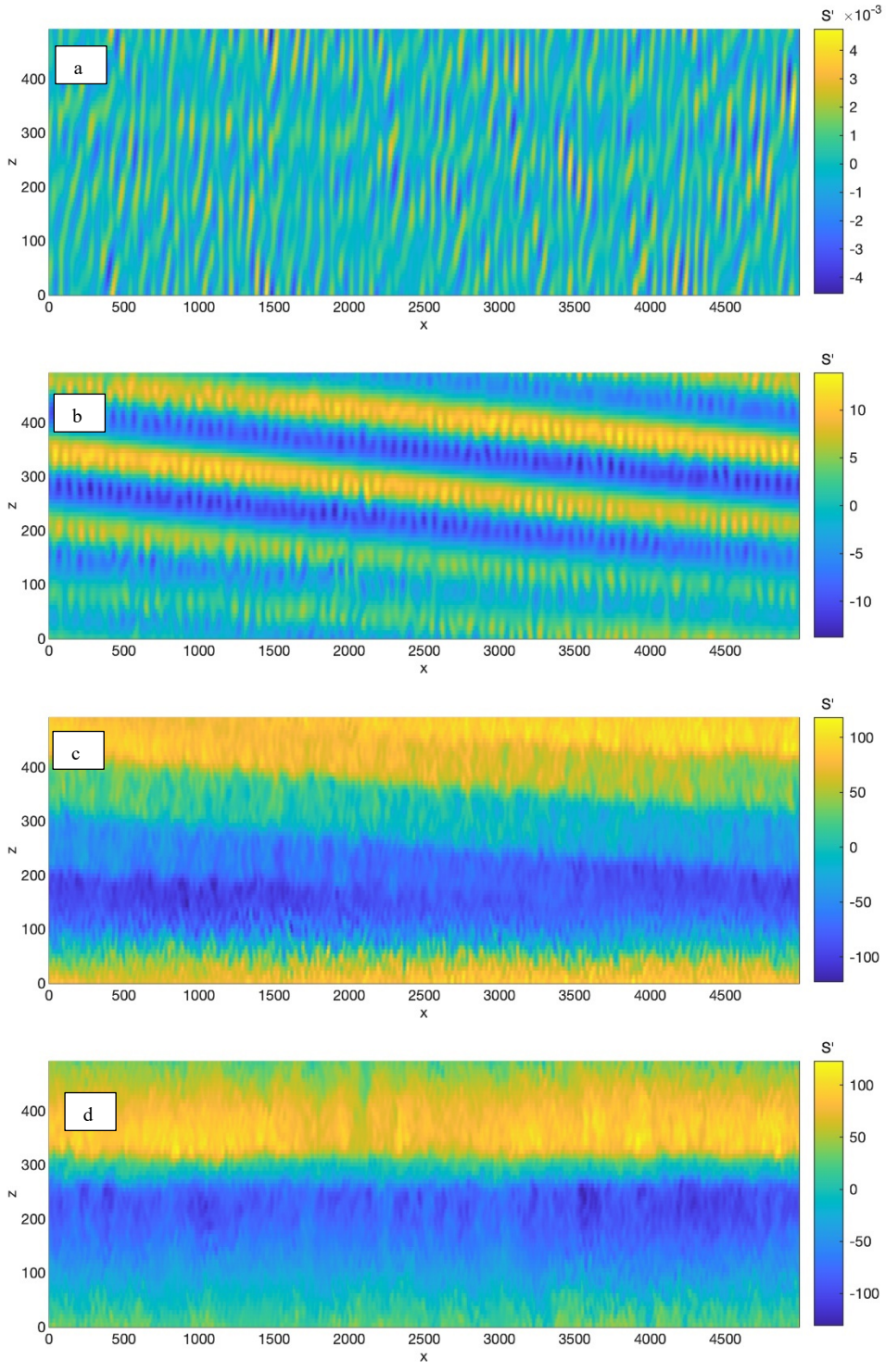

Figure 9. Evolutionary scenario one: Parameterized model salinity perturbation (x–z plane).

Figure 10 shows a simulation with G = .001, R_ρ=2 and A= 10, which evolves following the second scenario, in which the collective instability structures persist. Figure 10a-d displays the following simulation at t=91, t=302, t=412, and t=1500 in the same manner as Figure 9. As the slope of the isohalines and isotherms decreases, so too does the inclination of typical intrusive modes (Merryfield, 2000), and thus, to allow for at least one wavelength across the simulation, we are required to increase the domain size to 4000 by 40000. The salinity field again shows meter-scale instabilities developing at earlier times in Figure 10a,b. As time progresses, the collective instability begins to amplify internal waves in Figure 10c. Figure 10d shows these internal waves stabilizing and continuing to propagate through the domain. The difference in morphology between these cases is also expected to result in substantial effects on the net transport, with this case producing oscillating fluxes, as shown in Figure 11. Merryfield (2000) discusses that the growth rate of intrusive modes decreases proportionally to G, which would then suggest that it would take 100 times longer for intrusions to develop for G=0.001 than for the case in Figure 9. The fact that intrusions are not seen in Figure 10 does not preclude the possibility of their formation at later times. As such, it appears to be beyond even the ability of this parametric model to explore such values.

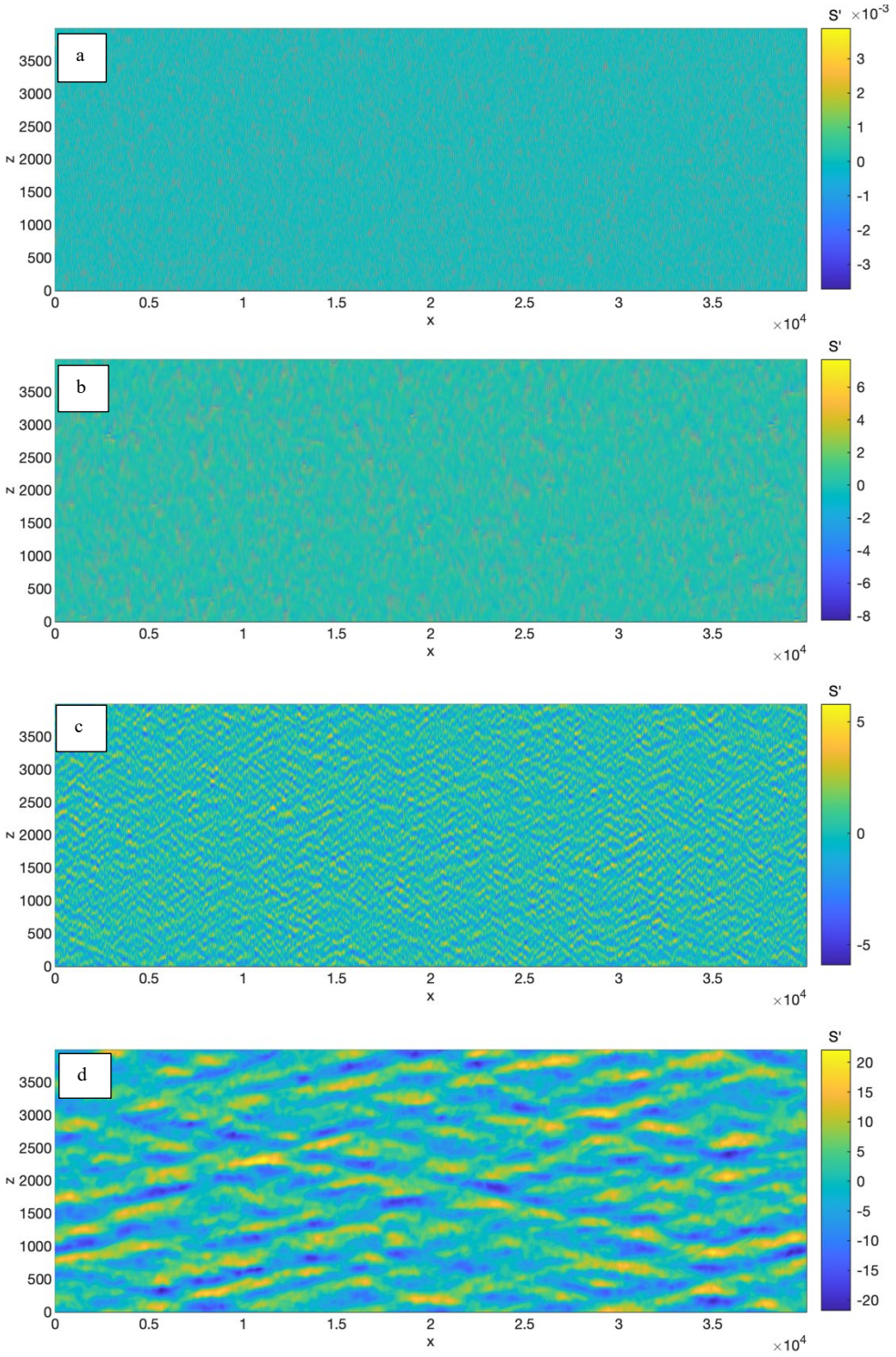

Figure 10. Evolutionary scenario two: Parameterized model salinity perturbation (*x*–*z* plane).

Figure 11 shows the time series of the vertical and horizontal salinity fluxes for simulations with a density ratio of 2, aspect ratio of 10, domain of 500 by 5000 and the isothermal slopes of 0.1, 0.01, and 0.001. Figure 12 shows us that at lower gradients, the growth of the instability is substantially decreased. Only the case with an isothermal slope of 0.1 develops substantial mixing. The periods of flux growth and collapse are likely due to the gradual development of a shear layer within the convective region of the staircases, which eventually grows until it temporarily disrupts the staircase interfaces. The cases with smaller isothermal slopes show no sign of nearing equilibration and appear to be dominated by oscillating collective modes.

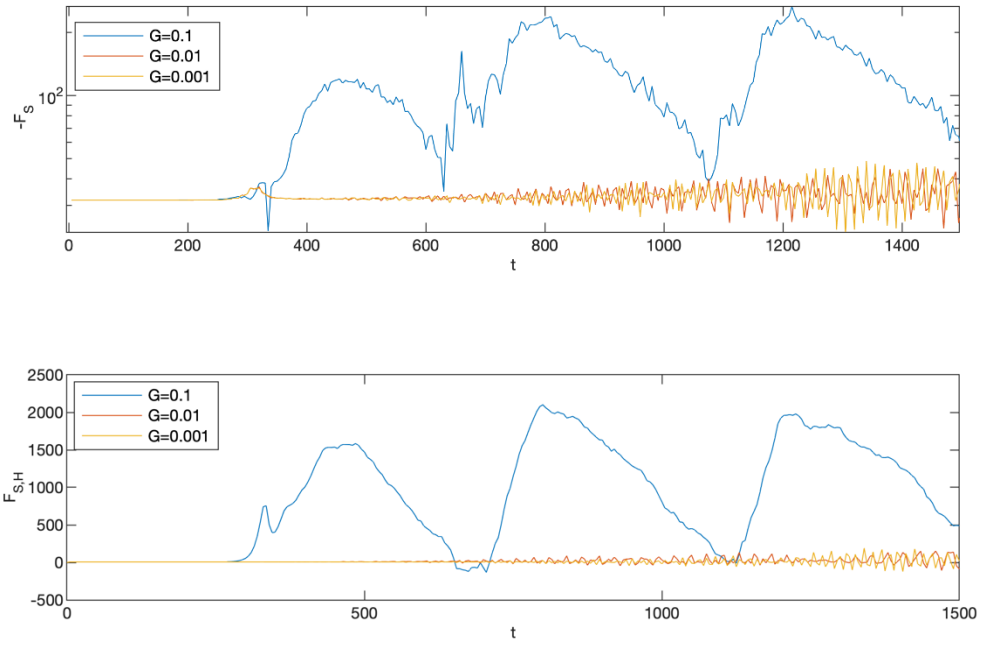

Figure 11. Parameterized model salinity vertical and horizontal fluxes comparison throughout time.

Figure 12 plots the salinity flux as a function of the isohaline isothermal slope for the parameterized simulations with R_ρ = 2 and A = 10, with a domain of 4000 by 40000 and 500 by 5000. This shows that there is a difference in both average vertical and horizontal fluxes when the gradient G goes increases from 0.01 to 0.03. The average fluxes increase from less than two in the vertical and less than 50 in the horizontal to values over

70 in the vertical and over 1100 in the horizontal. Larger gradients evolve into staircases likely due to the fact that the lower isothermal slope cases were unable to reach final equilibration by the end of the simulated time. Regarding the domains sizes, the smaller domains tends to have smaller average fluxes than the larger domains. This is attributed to the fact that large domains take into account a wider range of large-scale phenomena. In particular, all such simulations develop thermohaline staircases, the layers of which merge to form a single large-scale convection zone. Since the flux due to convection is proportional to the layer height to the 4/3 power (see, e.g., Linden, 2000), the final fluxes are correspondingly larger.

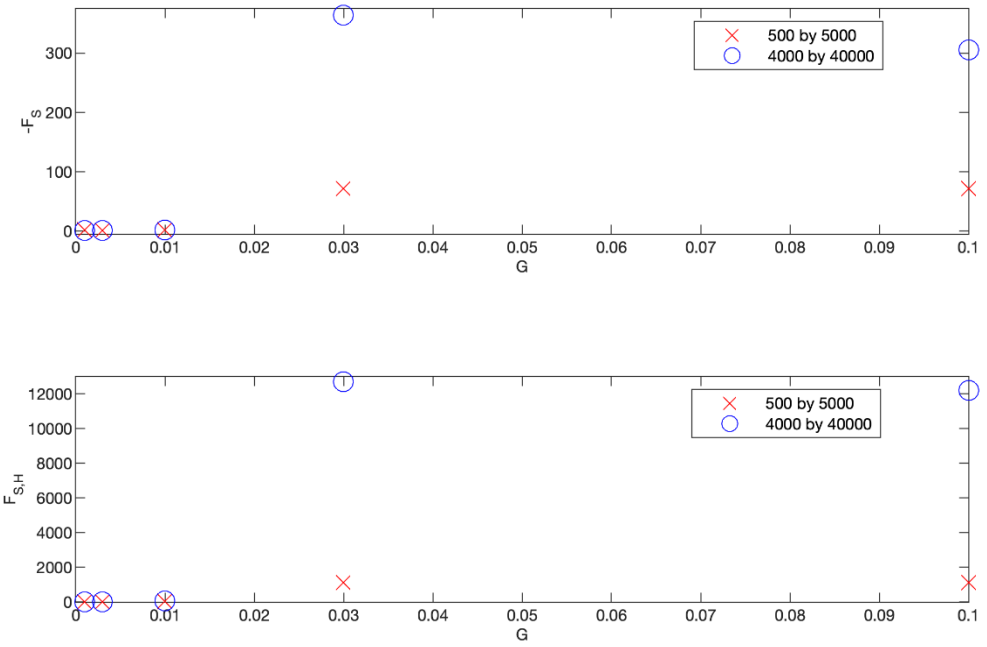

Figure 12. Parameterized vertical and horizontal flux in respect to gradient.

Table 3 lists the averaged quantities for all our parameterized model simulations and identifies which evolutionary scenario is present for each simulation. Based on Table 3, we are able to confirm that, for a density ratio of 2, when the isothermal slope is 0.03 or more, enough time has passed by t=1500 to allow for the development of direct intrusions, which eventually become thermohaline staircases. The average horizontal and vertical

fluxes are therefore much larger for these parameters, as the internal waves amplified by the collective instability cannot transport material as efficiently. For isothermal slopes less than 0.03 and for a density ratio of 2, the development of the intrusive instability is either too slow to develop by t=1500 or else otherwise forbidden by the parameter choices. For the cases with density ratios of 2.5 and 3, we instead find that such systems develop even more slowly and that it remains difficult to assess which evolutionary scenario is likely.

Table 3. Averaged fluxes and evolution for each parameterized model simulation.

R_ρ	A	G	$\overline{F_T}$	$\overline{F_S}$.	$\overline{F_{T,H}}$.	$\overline{F_{S,H}}$.	Scenario
2	5k x 500	0.1	-4.80E+01	-7.17E+01	1.39E+03	1.12E+03	1
2	40k x 4k	0.1	-1.50E+02	-3.06E+02	1.03E+04	1.22E+04	1
2	80k x 4k	0.1	-1.53E+02	-2.97E+02	8.85E+03	1.09E+04	1
2	5k x 500	0.01	-1.13E+00	-1.60E+00	6.18E+01	4.53E+01	2
2	40k x 4k	0.01	-1.34E+00	-1.86E+00	6.65E+01	5.43E+01	2
2.5	5k x 500	0.01	-6.40E-03	-9.40E-03	9.62E-05	4.14E-05	n/a
2.5	40k x 4k	0.01	5.32E-09	5.32E-09	6.78E-10	2.99E-10	2
3	5k x 500	0.01	-3.85E-02	-3.86E-02	-8.90E-03	-2.50E-03	n/a
3	40k x 4k	0.01	-3.27E-02	-3.28E-02	1.50E-03	2.20E-03	n/a
2	5k x 500	0.03	-4.80E+01	-7.17E+01	1.39E+03	1.12E+03	1
2	40k x 4k	0.03	-2.08E+02	-3.64E+02	1.12E+04	1.27E+04	1
2	5k x 500	0.001	-1.92E+00	-1.50E+00	2.04E+00	3.88E+00	2
2	40k x 4k	0.001	-5.88E-01	-8.16E-01	-1.62E+00	-1.97E-01	2
2	5k x 500	0.003	-8.73E-01	-1.25E+00	3.69E+00	4.72E+00	2
2	40k x 4k	0.003	-6.40E-01	-8.88E-01	1.13E+00	2.82E+00	2

V. CONCLUSION

A. DISCUSSION

This study was motivated by the need to better understand the lateral and vertical transport of intrusive processes. We used two-dimensional numerical simulations to model an ocean environment with inclined isotherms and isohalines to generate intrusive and collective instabilities and measured the transport of heat and salt in these systems. We have discovered that the lateral intrusion-driven transport depends sensitively on the density ratio. As the vertical mixing by salt fingers decreases with increasing density ratio, so do the vertical and lateral mixing of the intrusive and collective instabilities, which are driven by the microscale finger fluxes. The transport decreases with an increase in R_ρ because at higher density ratios the transport takes longer to develop and therefore fluxes are weaker. The simulations performed with higher aspect ratio A tend to become more affected by collective instabilities, which are characterized by stronger oscillations and lower transport. In our fully resolved simulations, we measured the small-scale mixing in 25-cm regions. We then compared our DNS-based results to the predictions of previous mixing models, such as Radko and Smith (2012) for salt fingers, Kelly (1990) for diffusive convection, Ellison and Turner (1959) and Xu et al. (2006) for shear turbulence, and Linden (2000) for convective turbulence. We found substantial disagreement between the models and the measured fluxes within the intrusive environment, which calls into question their ability to represent such phenomena.

We found that strong isothermal slopes, those that are possible to simulate numerically, tend to form collective instabilities initially rather than direct intrusions. The growth rate of this instability decreases significantly as the density ratio increases. In addition, the period of the collective instability oscillations depends linearly on the buoyancy frequency, which is related to the density ratio. We found through numerical simulations that collective instabilities are the preferred initial development. Such a result is not possible in a study like that of Simeonov and Stern (2007) where the tilt of the simulation was prescribed. This does not preclude the possibility of the eventual formation of direct intrusions or thermohaline staircases.

We used prior prescriptions for the mixing due to double-diffusive processes to act as a sub-grid scale mixing model in a series of simulations with coarse (~25cm) resolution. We performed a series of such simulations at parameters that would be difficult or impossible to simulate with full resolution and found that large, fingering-unstable regions with horizontal gradients of temperature and salinity develop in two different evolutionary scenarios. The first scenario develops direct-mode intrusions and eventually evolves into thermohaline staircases, and the second scenario develops internal waves which are amplified by the collective instability. Since direct intrusion modes would take much longer to develop as G decreases, at lower G, the collective instability (which doesn't depend on G) is more evident. This suggests a few possibilities. In one case, intrusions develop directly, and in such cases, we always see the development of thermohaline staircases. The second scenario is the development of the collective instability with no sign of direct intrusions. We suspect that many such cases would develop intrusions eventually, but it is also possible that, under certain parameters, direct intrusions may be prohibited.

B. FUTURE STUDIES

Although the parameterized model provides qualitative agreement by producing collective and intrusive instabilities, ensuring that it can reproduce such behaviors for a large span of parameter space would be critically important. Such model development would benefit from comparisons with more numerical simulations and also from laboratory and observational work. In addition, a three-dimensional model may be developed to more accurately represent the transport of salt and heat in the ocean. A 3D model can be calibrated using known three-dimensional microstructure flux laws.

Running a more extensive array of parameterized simulations would make it possible to develop an analytic prescription for the large-scale mixing caused by intrusions in the ocean. Such a prescription would be of substantial interest to the larger ocean-modeling community to ensure that the effects of intrusions are accounted for in future oceanic studies and predictions. This would provide a greater capacity to more accurately predict weather patterns and global climate.

Furthermore, from a tactical naval standpoint, the acoustic transmission loss through such structures can be measured by inputting the model output from this study into an acoustic ray-tracing software such as BELLHOP. Such analysis could aid in determining the presence of acoustic blind spots in an environment where intrusions are present. Such a study could be further enhanced through an operational study of target detection and acoustic transmission in such regions of the ocean.

THIS PAGE INTENTIONALLY LEFT BLANK

LIST OF REFERENCES

Armi, L., D. Hebert, N. Oakey, J. Price, P. L. Richardson, T. Rossby, and B. Ruddick, 1988: The history and decay of a Mediterranean salt lens. *Nature*, **333**, 649–651, https://doi.org/10.1038/333649a0.

Bell, J. H., and R. D. Mehta, 1990: Development of a two-stream mixing layer from tripped and untripped boundary layers. *AIAA Journal*, **28**, 2034–2042, https://doi.org/10.2514/3.10519.

Canuto, C., M. Hussaini, A. Quarteroni, and T. Zang, 2007: *Spectral Methods: Evolution to Complex Geometries and Applications to Fluid Dynamics*. Springer Science & Business Media.

Ellison, T. H., and J. S. Turner, 1959: Turbulent entrainment in stratified flows. *J. Fluid Mech.*, **6**, 423, https://doi.org/10.1017/S0022112059000738.

Glessmer, M. S., A. Oschlies, and A. Yool, 2008: Simulated impact of double-diffusive mixing on physical and biogeochemical upper ocean properties. *J. Geophys. Res.*, **113**, C08029, https://doi.org/10.1029/2007JC004455.

Greenert, J., 2014: *The United States Navy Arctic Roadmap for 2014 to 2030.* Office of the Chief of Naval Operations Washington, DC.

Hansen, J., and Coauthors, 2007: Dangerous human-made interference with climate: a GISS modelE study. *Atmos. Chem. Phys.*, **7**, 2287–2312, https://doi.org/10.5194/acp-7-2287-2007.

Hebert, M., 2011: Numerical simulations, mean field theory and modulational stability analysis of thermohaline intrusions. Dept. of Meteorology, Naval Postgraduate School. http://hdl.handle.net/10945/5582.

Huppert, H. E., and J. S. Turner, 1980: Ice blocks melting into a salinity gradient. *J. Fluid Mech.*, **100**, 367, https://doi.org/10.1017/S0022112080001206.

Joyce, T. M., W. Zenk, and J. M. Toole, 1978: The anatomy of the Antarctic polar front in the Drake Passage. *J. Geophys. Res.*, **83**, 6093, https://doi.org/10.1029/JC083iC12p06093.

Kelley, D., 1984: Effective diffusivities within oceanic thermohaline staircases. *J. Geophys. Res.*, **89**, 10484, https://doi.org/10.1029/JC089iC06p10484.

Kelley, D. E., 1988: Explaining effective diffusivities within diffusive oceanic staircases. *Elsevier Oceanography Series*, Vol. 46 of, Elsevier, 481–502.

——, 1990: Fluxes through diffusive staircases: A new formulation. *J. Geophys. Res.*, **95**, 3365, https://doi.org/10.1029/JC095iC03p03365.

Krishnamurti, R., 2009: Heat, salt and momentum transport in a laboratory thermohaline staircase. *J. Fluid Mech.*, **638**, 491–506, https://doi.org/10.1017/S002211200999098X.

Large, W. G., J. C. McWilliams, and S. C. Doney, 1994: Oceanic vertical mixing: A review and a model with a nonlocal boundary layer parameterization. *Rev. Geophys.*, **32**, 363, https://doi.org/10.1029/94RG01872.

Linden, P. F., 1974: Salt fingers in a steady shear flow. *Geophys. Fluid Dynamics*, **6**, 1–27, https://doi.org/10.1080/03091927409365785.

McLaughlin, F. A., E. C. Carmack, R. W. Macdonald, H. Melling, J. H. Swift, P. A. Wheeler, B. F. Sherr, and E. B. Sherr, 2004: The joint roles of Pacific and Atlantic-origin waters in the Canada Basin, 1997–1998. *Deep Sea Research Part I: Oceanographic Research Papers*, **51**, 107–128, https://doi.org/10.1016/j.dsr.2003.09.010.

McLaughlin, F. A., E. C. Carmack, W. J. Williams, S. Zimmermann, K. Shimada, and M. Itoh, 2009: Joint effects of boundary currents and thermohaline intrusions on the warming of Atlantic water in the Canada Basin, 1993–2007. *J. Geophys. Res.*, **114**, C00A12, https://doi.org/10.1029/2008JC005001.

Merryfield, B., 2005: Ocean mixing in 10 steps. *Science*, **308**, 641–642, https://doi.org/10.1126/science.1111417.

Merryfield, W. J., 2000: Origin of thermohaline staircases. *J. of Phys. Oceanogr.*, **30**, 1046–1068, https://doi.org/10.1175/1520-0485(2000)030<1046:OOTS>2.0.CO;2.

Merryfield, W. J., and O. A. Saenko, 2005: On the effect of topographically enhanced mixing on the global ocean circulation. *J. of Phys. Oceanogr.,* **35**, 826–834, https://doi.org/10.1175/JPO2722.1.

Mueller, R. D., W. D. Smyth, and B. Ruddick, 2007: Shear and Convective Turbulence in a Model of Thermohaline Intrusions. *J. of Phys. Oceanogr.,* **37**, 2534–2549, https://doi.org/10.1175/JPO3137.1.

Peyret, R., 2002: *Spectral Methods for Incompressible Viscous Flow*. Springer Science & Business Media.

Pope, S., 2000: *Turbulent Flows*. Cambridge University Press.

Radko, T., 2005: What determines the thickness of layers in a thermohaline staircase? *J. Fluid Mech.*, **523**, 79–98, https://doi.org/10.1017/S0022112004002290.

——, 2013: *Double-Diffusive Convection*. Cambridge University Press.

——, 2014: Applicability and failure of the flux-gradient laws in double-diffusive convection. *J. Fluid Mech.*, **750**, 33–72, https://doi.org/10.1017/jfm.2014.244.

——, and D. P. Smith, 2012: Equilibrium transport in double-diffusive convection. *J. Fluid Mech.*, **692**, 5–27, https://doi.org/10.1017/jfm.2011.343.

——, and C. Sisti, 2017: Life and demise of intrathermocline mesoscale vortices. *J. of Phys. Oceanogr.*, **47**, 3087–3103, https://doi.org/10.1175/JPO-D-17-0044.1.

Rogers, M. M., and R. D. Moser, 1994: Direct simulation of a self-similar turbulent mixing layer. *Physics of Fluids*, **6**, 903–923, https://doi.org/10.1063/1.868325.

Ruddick, B., and K. Richards, 2003: Oceanic thermohaline intrusions: observations. *Progress in Oceanogr.*, **56**, 499–527, https://doi.org/10.1016/S0079-6611(03)00028-4.

Ruddick, B. R., 1985: Momentum transport in thermohaline staircases. *J. Geophys. Res.*, **90**, 895, https://doi.org/10.1029/JC090iC01p00895.

Ruddick, B. R., and J. S. Turner, 1979: The vertical length scale of double-diffusive intrusions. *Deep Sea Research Part A. Oceanographic Research Papers*, **26**, 903–913, https://doi.org/10.1016/0198-0149(79)90104-3.

Ruddick, B. R., O. M. Phillips, and J. S. Turner, 1999: A laboratory and quantitative model of finite-amplitude thermohaline intrusions. *Dynamics of Atmospheres and Oceans*, **30**, 71–99, https://doi.org/10.1016/S0377-0265(99)00021-4.

Rudels, B., 2009: Arctic Ocean Circulation. *Encyclopedia of Ocean Sciences*, Elsevier, 211–225.

Schmitt, R. W., and D. T. Georgi, 1982: Finestructure and microstructure in the North Atlantic Current. *J. Mar. Res.*, **40,** 659–705.

Shen, C. Y., 1995: Equilibrium salt-fingering convection. *Physics of Fluids*, **7**, 706–717, https://doi.org/10.1063/1.868596.

Simeonov, J., and M. E. Stern, 2007: Equilibration of Two-Dimensional Double-Diffusive Intrusions. *J. of Phys. Oceanogr.*, **37**, 625–643, https://doi.org/10.1175/JPO3000.1.

Smyth, W. D., and J. N. Moum, 2000: Length scales of turbulence in stably stratified mixing layers. *Physics of Fluids*, **12**, 1327–1342, https://doi.org/10.1063/1.870385.

Stellmach, S., A. Traxler, P. Garaud, N. Brummell, and T. Radko, 2011: Dynamics of fingering convection. Part 2 The formation of thermohaline staircases. *J. Fluid Mech.*, **677**, 554–571, https://doi.org/10.1017/jfm.2011.99.

Stern, M. E., 1960: The "salt-fountain" and thermohaline convection. *Tellus*, **12**, 172–175, https://doi.org/10.3402/tellusa.v12i2.9378.

——, 1967: Lateral mixing of water masses. *Deep Sea Research and Oceanographic Abstracts*, **14**, 747–753, https://doi.org/10.1016/S0011-7471(67)80011-1.

Tanny, J., and A. B. Tsinober, 1988: The dynamics and structure of double-diffusive layers in sidewall-heating experiments. *J. Fluid Mech.*, **196**, 135–156, https://doi.org/10.1017/S0022112088002642.

Thorpe, S. A., P. K. Hutt, and R. Soulsby, 1969: The effect of horizontal gradients on thermohaline convection. *J. Fluid Mech.*, **38**, 375–400, https://doi.org/10.1017/S0022112069000231.

Traxler, A., S. Stellmach, P. Garaud, T. Radko, and N. Brummell, 2011: Dynamics of fingering convection. Part 1 Small-scale fluxes and large-scale instabilities. *J. Fluid Mech.*, **677**, 530–553, https://doi.org/10.1017/jfm.2011.98.

Turner, J. S., 1978: Double-diffusive intrusions into a density gradient. *J. Geophys. Res.*, **83**, 2887, https://doi.org/10.1029/JC083iC06p02887.

——, and C. F. Chen, 1974: Two-dimensional effects in double-diffusive convection. *J. Fluid Mech.*, **63**, 577–592, https://doi.org/10.1017/S0022112074001790.

Walsh, D., and B. Ruddick, 1998: Nonlinear equilibration of thermohaline intrusions. *Journal of Physical Oceanography*, **28**, 1043–1070, https://doi.org/10.1175/1520-0485(1998)028<1043:NEOTI>2.0.CO;2.

——, and E. Carmack, 2002: A note on evanescent behavior of Arctic thermohaline intrusions. *J. of Marine Res.*, **60**, 281–310, https://doi.org/10.1357/002224002760497499.

Williams, A. J., 1981: The role of double diffusion in a Gulf Stream frontal intrusion. *J. Geophys. Res.*, **86**, 1917–1928, https://doi.org/10.1029/JC086iC03p01917.

Xu, X., Y. S. Chang, H. Peters, T. M. Özgökmen, and E. P. Chassignet, 2006: Parameterization of gravity current entrainment for ocean circulation models using a high-order 3D nonhydrostatic spectral element model. *Ocean Modelling*, **14**, 19–44, https://doi.org/10.1016/j.ocemod.2006.02.006.

INITIAL DISTRIBUTION LIST

1. Defense Technical Information Center
   Ft. Belvoir, Virginia

2. Dudley Knox Library
   Naval Postgraduate School
   Monterey, California